The metal - insulator transition in $NdNi_{1-x}Cu_xO_3$ perovskites

1996 J. Phys.: Condens. Matter 8 10393

(http://iopscience.iop.org/0953-8984/8/49/028)

J. Phys.: Condens. Matter **8** (1996) 10393–10405. Printed in the UK

The metal–insulator transition in $NdNi_{1-x}Cu_xO_3$ perovskites

J Pérez†, J Stankiewicz†, J Blasco†, M Castro†‡ and J García†§

† Instituto de Ciencia de Materiales de Aragón, Centro Superior de Investigaciones Científicas, Universidad de Zaragoza, 50009 Zaragoza, Spain

‡ Departamento de Ciencia de Materiales, Centro Politécnico Superior, Universidad de Zaragoza, 50015 Zaragoza, Spain

Received 16 July 1996

Abstract. The perovskite oxides $NdNi_{1-x}Cu_xO_3$ have been synthesized for $0 \leqslant x \leqslant 0.2$ under high oxygen pressure using a sol–gel method. Their structural, electrical, magnetic and calorimetric properties have been measured over a wide temperature range (4–300 K). All of the samples have an orthorhombic unit cell which does not change with Cu content. Nevertheless, their electrical properties change drastically with x from the very lowest values of x. The metal–insulator transition temperature decreases as x increases, up to $x = 0.03$; for $x \geqslant 0.03$ the system is metallic for all temperatures. Moreover, the replacing of Ni with Cu atoms leads to magnetic disorder in the Ni sublattice.

1. Introduction

Metal–insulator (MI) transitions in mixed transition metal and rare-earth oxides have been studied for a long time [1]. The discovery of new properties of these materials, such as high-temperature superconductivity and colossal magnetoresistance, has renewed interest in them. The electronic structure of 3d transition metal oxides is usually described by the Zaanen, Sawatzky and Allen (ZSA) scheme [2] in which a relationship between the 3d–3d Coulomb repulsion energy, U, and the ligand-to-metal charge-transfer energy, Δ, is considered. In this scheme, the transition metal compounds are divided into two classes: the Mott–Hubbard and the charge-transfer compounds. In the Mott–Hubbard materials, U is smaller than Δ and the magnitude of the band gap is given by U. In the charge-transfer compounds, $\Delta < U$ and the magnitude of the gap is given by Δ. It has been shown that some high-valence transition metal oxides have small or negative Δ [3]. These oxides have been classified as covalent metals or insulators. Their band gap is then determined by the hybridization between the transition metal 3d and oxygen 2p orbitals. Its magnitude is strongly affected by the geometrical arrangement of the transition metal and oxygen ions, and a small lattice distortion may cause a MI transition in these compounds.

$RENiO_3$ (RE: rare earth) mixed oxides are of special interest since they exhibit a temperature-driven MI transition [4]. $LaNiO_3$ is a semimetal whose current carriers are highly correlated [5]. Oxides with smaller rare-earth ions (Pr, Nd, Sm and Eu) show a MI transition whose temperature increases as the rare-earth-ion size decreases. All of these oxides show a large mixing of nickel 3d and oxygen 2p orbitals in the ground state [3, 6].

§ Author to whom any correspondence should be addressed.

0953-8984/96/4910393+13$19.50

Moreover, the MI transition is accompanied by an expansion of the unit cell in the insulating phase together with a decrease of the Ni–O–Ni bond angle. The latter governs the transfer integral for Ni 3d and O 2p orbitals [7]. In addition, a simultaneous antiferromagnetic arrangement of the Ni sublattice is observed when RE = Pr and Nd, while the magnetic transition occurs below the MI transition temperature for Sm and Eu compounds [4]. The magnetic ordering has a propagation vector $\boldsymbol{k} = (1/2, 0, 1/2)$, related to an orbital momentum superlattice that arises from strong intra-atomic Coulomb correlations [8].

The MI transition in nickel perovskite oxides is affected by hole and electron doping [9], and also by partial substitution for Ni with other transition metals [10]. A preliminary study has shown that the electrical properties of $NdNi_{1-x}Cu_xO_3$ ($x = 0.05$, 0.1 and 0.15) change strongly with copper content [11]. However, the properties of these materials are also very sensitive to oxygen deficiency. All of the samples studied previously have been prepared by sintering at low temperatures, and have been oxygen deficient. Consequently, their electronic properties were altered not only by replacement of Ni with Cu atoms but also by the change in the number of oxygen vacancies.

In this paper we report results of structural, magnetic, electrical, and calorimetric studies of $NdNi_{1-x}Cu_xO_3$ ($x \leqslant 0.2$) stoichiometric samples. Special care has been taken in the preparation of these compounds in order to ensure the correct compositions. Our aim was to study in detail how the magnetic and electrical transport properties vary with partial substitution for Ni with Cu. New data are presented which cast some light on the origin and mechanism of the MI transition in $RENiO_3$ compounds.

2. Experimental details

Samples were prepared by a citrate route and thermal treatment under an oxygen pressure of 200 bars. Stoichiometric amounts of Nd_2O_3, CuO and $2NiCO_33Ni(OH)_2{\cdot}4H_2O$ were dissolved in nitric acid. After addition of citric acid and ethylene glycol in the appropriate ratio [12], the solutions were heated until green-blue gels were formed. These gels were dried to obtain brown powders which, in turn, were calcined overnight by immersion in oxygen flowing at 500 °C. The resulting black powders were pressed (4–5 kbar) and sintered at 900 °C, under oxygen pressure of 200 bar for 12 h.

The amount of oxygen content in the samples was determined from thermogravimetric curves obtained using a TGA system working at a heating rate of 5 °C min^{-1} in a reducing flow of N_2:H_2 (95:5). The composition of samples was determined using a Jeol JSM-6400 electron microscope and Analytical Link EDS x-ray spectrometer. Polished bulk samples were used for this purpose. The Nd:Ni:Cu atomic ratio obtained agreed with the nominal values for all of the samples studied.

X-ray powder diffraction (XRD) patterns were collected using a D-max Rigaku system with a rotating anode operating at 40 kV and 100 mA. The Cu Kα radiation was selected using a graphite monochromator. The diagrams were obtained by a step scanning of the angle 2θ from 19° up to 140° with a step size of 0.02°, and with a counting time of 10 s/step for structural refinements. X-ray diffraction patterns were analysed by the Rietveld method with the FULLPROF program [13]. A pseudo-Voigt function was used as the diffraction peak shape function.

Magnetic measurements were carried out between 4.2 and 300 K in a commercial Quantum Design (SQUID) magnetometer. Resistance measurements were performed using the standard six-probe AC method in the temperature range 4 to 300 K. Magnetoresistance measurements were carried out in fields of up to 12 T.

Thermal expansion was measured between 130 K and 375 K by a 'push rod' method.

Heat capacity data were obtained using an AC calorimeter (ACC1-VL Sinku-Riko) in the temperature range 5 to 250 K. In addition, a differential scanning calorimeter (Perkin–Elmer) was used to obtain data near room temperature.

3. Results

3.1. Structural details

$NdNi_{1-x}Cu_xO_3$ samples with $x \leqslant 0.2$ have been prepared by the procedure described in the previous section. Our attempts to increase the Cu content were unsuccessful; they gave rise to new peaks in the diffraction patterns corresponding to Nd_2MO_4 phases (M = Ni, Cu). This shows that higher oxygen pressure is needed in order to increase the degree of substitution of Cu atoms for Ni as has been reported for the synthesis of $NdCuO_{3-\delta}$ [14].

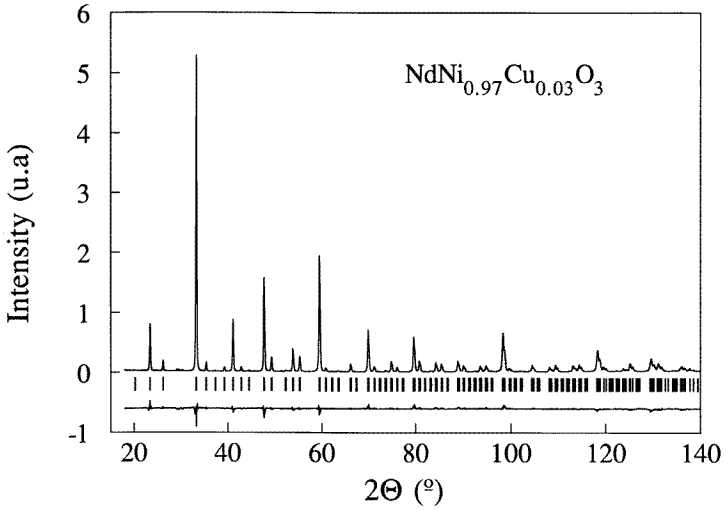

Figure 1. Experimental (points) and calculated (line) x-ray diffraction patterns for $NdNi_{0.97}Cu_{0.03}O_3$ at room temperature. The difference between the experimental and calculated patterns is plotted at the bottom and the bars (|) denote the calculated Bragg reflection positions.

The XRD patterns of $NdNi_{1-x}Cu_xO_3$ samples show the same single-phase crystallographic structure for the whole series. Only for $x = 0.2$ have some minor peaks from impurity phases been detected. At room temperature, all of the samples have the orthorhombic $GdFeO_3$ structure that is well described by the *Pbnm* spatial group (D_{16}^h). The atoms are placed at the following Wyckoff positions: Nd at 4c: $(x, y, 1/4)$; the transition metal (Ni or Cu) at 4b: $(1/2, 0, 0)$; and two inequivalent oxygens, O(1) at 4c: $(x, y, 1/4)$ and O(2) at 8d: (x, y, z). Since we have not observed additional diffraction peaks, we can conclude that Cu replaces Ni at random. Figure 1 shows one of the fitted diffraction patterns for $NdNi_{0.97}Cu_{0.03}O_3$. The final refined unit cell and atomic positions are listed in table 1 together with the conventional Rietveld reliability parameters. The low values of these parameters show the accuracy of the assumed structure. The results obtained for pure $NdNiO_3$ are in excellent agreement with neutron diffraction data reported earlier [7]. The values for Ni and Cu contents obtained from refinement analysis are equal to the nominal values. These values have also been confirmed by fluorescence analysis. The homogeneity

Table 1. Refined fractional atomic positions, unit cells and reliability factors (%) for $NdNi_{1-x}Cu_xO_3$ at room temperature ($Z = 4$). Nd and O(1) are located at (4c): $(x, y, 1/4)$. The transition metal (Ni or Cu) is at (4b): $(1/2, 0, 0)$. An overall Debye–Waller factor of $B = 0.3$ Å^2 has been fixed for all atoms.

		$x = 0$	$x = 0.01$	$x = 0.02$	$x = 0.03$	$x = 0.05$	$x = 0.1$	$x = 0.2$
Nd:								
	x:	0.9944(2)	0.9947(2)	0.9943(2)	0.9944(3)	0.9945(2)	0.9945(2)	0.9969(2)
	y:	0.0351(1)	0.0353(1)	0.0354(1)	0.0354(1)	0.0356(1)	0.0355(1)	0.0356(1)
O(1):								
	x:	0.070(1)	0.074(3)	0.073(3)	0.073(3)	0.077(3)	0.076(2)	0.083(2)
	y:	0.490(1)	0.493(1)	0.492(1)	0.494(1)	0.495(1)	0.494(1)	0.494(1)
O(2):								
	x:	0.712(1)	0.713(1)	0.713(1)	0.714(1)	0.715(1)	0.714(1)	0.709(2)
	y:	0.284(1)	0.282(1)	0.284(1)	0.283(1)	0.283(1)	0.281(1)	0.285(2)
	z:	0.036(1)	0.035(1)	0.036(1)	0.036(1)	0.035(1)	0.035(1)	0.032(1)
a (Å):		5.3903(1)	5.3889(1)	5.3900(1)	5.3896(1)	5.3898(1)	5.3936(1)	5.3962(1)
b (Å):		5.3807(1)	5.3808(1)	5.3823(1)	5.3828(1)	5.3842(1)	5.3837(1)	5.3870(1)
c (Å):		7.6100(2)	7.6095(1)	7.6109(2)	7.6109(1)	7.6117(2)	7.6136(1)	7.6163(1)
R_{wp}:		10.2	9.9	8.8	9.4	9.4	8.6	7.4
R_{exp}:		4.0	3.3	3.9	3.8	3.6	3.4	2.8
χ^2:		6.3	8.9	8.0	6.2	6.7	6.3	6.8
R_B:		5.4	5.6	5.7	5.5	5.7	5.4	4.0

of the samples was checked with a transmission electron microscope.

As the Cu content in $NdNi_{1-x}Cu_xO_3$ increases, so does the unit-cell volume, as can be seen in table 1. This is in agreement with the reported values for $RENiO_3$ and $RECuO_3$ (RE = La, Nd) unit-cell parameters [14, 15]. The amount of oxygen in $NdNi_{1-x}Cu_xO_{3-\delta}$ samples, obtained by TGA, lies in the range $-0.02 \leqslant \delta \leqslant 0.03$. Therefore, our samples can be treated as stoichiometric. The calculated density, taking into account the slight unit-cell increase, is about 7.56 g cm^{-3} for all of the samples.

The distances and angles of the MO_6 (M = Ni, Cu) octahedron, calculated from the data of table 1, are given in table 2. All of the Ni–O distances are approximately equal and all of the values of the O–Ni–O angles are close to 90°. Therefore, the MO_6 octahedra are undistorted. The average M–O distance is about 1.942 Å except for the $x = 0.2$ sample where it is about 1.947 Å. The values of the Ni–O–Ni angle given in table 2 are nearly the same over the whole series. Therefore, the partial substitution for Ni with Cu produces minor and unimportant changes in the crystallographic structure of $NdNiO_3$.

3.2. Electrical transport properties

Figure 2 shows how the resistivity of the $NdNi_{1-x}Cu_xO_3$ samples ($x \leqslant 0.2$) varies with temperature in the range $4 \leqslant T \leqslant 300$ K. Normalized resistivities are plotted in the inset of figure 2. Samples with $x < 0.03$ show a sharp MI transition with large thermal hysteresis. The resistivity increases at the transition by several orders of magnitude. However, its value depends on preparation details and can vary from sample to sample. Clearly, the MI transition temperature strongly decreases with increasing Cu content, as has been previously reported [11], and the resistivity in the insulating phase becomes smaller with increasing x. The temperature of the MI transition decreases with x at a rate of about -4060 K/x. A

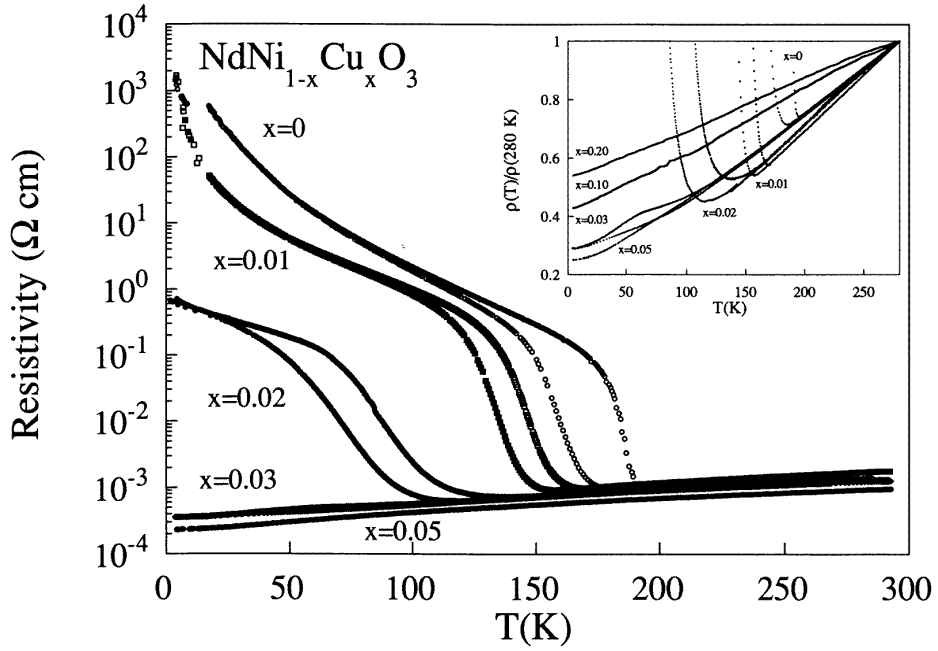

Figure 2. Resistivity versus temperature curves for $NdNi_{1-x}Cu_xO_3$ ($x \leqslant 0.2$) samples. The normalized resistivities are shown in the inset.

Table 2. Interatomic distances (Å) and angles (deg) for the M–O octahedron (M = Ni, Cu) of $NdNi_{1-x}Cu_xO_3$ at room temperature.

	No	$x = 0$	$x = 0.01$	$x = 0.02$	$x = 0.03$	$x = 0.05$	$x = 0.1$	$x = 0.2$
M–O(1):								
	2	1.941(3)	1.944(3)	1.943(3)	1.943(2)	1.948(2)	1.948(1)	1.956(1)
M–O(2):								
	2	1.928(8)	1.925(7)	1.932(7)	1.928(7)	1.933(7)	1.923(7)	1.922(9)
	2	1.958(8)	1.956(7)	1.953(7)	1.955(7)	1.947(7)	1.957(7)	1.964(9)
⟨M–O⟩:		1.942	1.942	1.942	1.942	1.943	1.942	1.947
O(1)–M–O(2):								
	2	89.8(5)	89.0(5)	89.5(3)	89.3(4)	89.6(4)	88.6(4)	87.0(5)
	2	89.8(5)	89.9(5)	90.0(4)	89.8(4)	89.9(5)	89.7(5)	88.7(5)
	2	90.2(6)	90.1(5)	90.0(3)	90.2(4)	90.1(5)	90.3(5)	91.3(5)
	2	90.2(5)	91.0(6)	90.5(4)	90.7(5)	90.4(5)	91.4(5)	93.0(6)
O(2)–M–O(2):								
	2	88.9(6)	88.9(5)	88.9(5)	88.9(5)	88.9(5)	89.0(5)	89.2(6)
	2	91.1(6)	91.1(5)	91.1(5)	91.1(5)	91.1(5)	91.0(5)	90.8(6)
M–O(1)–M:								
	2	157.2(6)	156.1(7)	156.6(6)	156.5(4)	155.1(5)	155.6(5)	153.5(5)
M–O(2)–M:								
	4	157.1(16)	157.6(16)	157.3(15)	157.5(15)	158.0(15)	158.2(15)	157.6(19)
⟨M–O–M⟩:		157.1	157.1	157.1	157.2	157.0	157.3	156.2

similar value has been found for hole-doped $RE_{1-x}A_xNiO_3$ perovskites [16]. The sample with $x = 0.03$ is metallic over the whole temperature range although its resistivity shows

a thermal hysteresis at low temperatures. This may be attributed to the existence of two metallic-like phases, with different electrical resistivities as has been proposed for $La_{1-x}Nd_xNiO_3$ [17] and for $PrNiO_3$ [18]. The samples with $x > 0.03$ show metallic behaviour. At low temperatures, $\rho(T) = \rho_0 + AT^2$, where the residual resistivity, ρ_0, varies between 0.17 and 0.68 mΩ cm as x changes from 0.05 to 0.2. For the $x = 0.05$ sample, $A = 3 \times 10^{-2}$ mΩ cm. The T^2-term in the resistivity may arise from electron–electron scattering. At high temperatures, the resistivity varies linearly with temperature for all samples studied. This is due to phonon–electron scattering. The slope of ρ versus T decreases slightly as x increases.

We did not find any systematic dependence of the residual resistivity on Cu content although $\Delta\rho(300\ \mathrm{K}) = [\rho(300\ \mathrm{K}) - \rho_0']/\rho_0'$ does correlate with x. Here, ρ_0' is the value of ρ obtained by an extrapolation of the high-temperature linear part of the resistivity to $T = 0$ K. $\Delta\rho(300\ \mathrm{K})$ decreases from a value of 7 in $NdNiO_3$ to a value of 4 in the $x = 0.03$ sample. The latter value is close to the one reported for $LaNiO_3$ [4, 19]. For higher Cu content, $\Delta\rho(300\ \mathrm{K})$ decreases to 0.9.

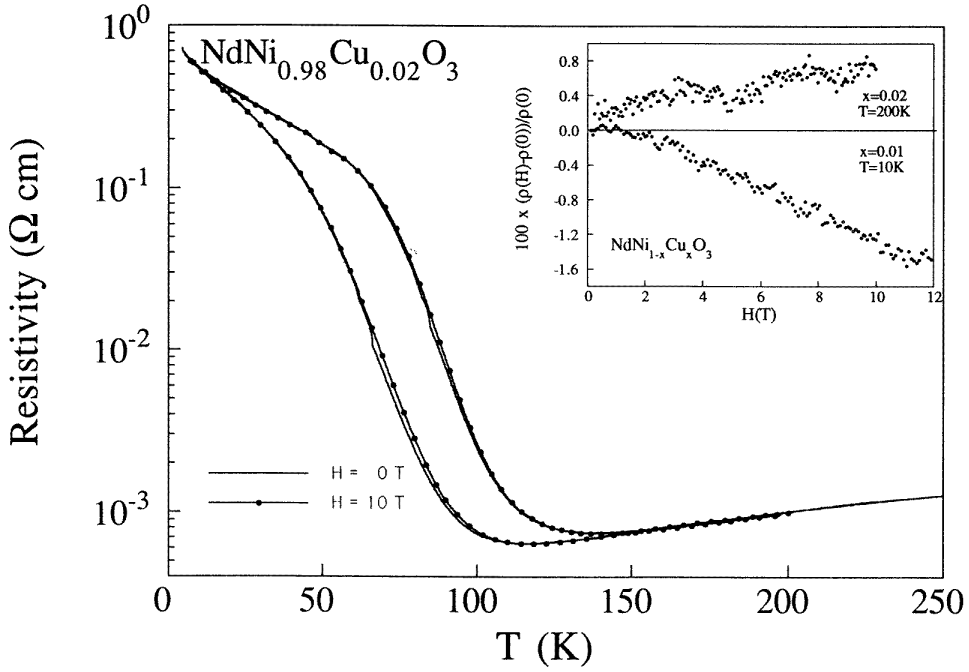

Figure 3. The resistivity versus temperature curve for the $NdNi_{0.98}Cu_{0.02}O_3$ sample in magnetic fields of 0 and 10 T. The inset shows the magnetoresistance curves for the $x = 0.02$ sample at 200 K and for $x = 0.01$ sample at 10 K.

Figure 3 shows resistivity versus temperature curves of the $x = 0.02$ sample under magnetic fields of 0 and 12 T. The two curves are almost identical and no changes are observed either in the shape of the MI transition or in the absolute values. Such behaviour suggests that no ferromagnetic polarons are formed in $NdNi_{1-x}Cu_xO_3$ contrary to the earlier hypothesis [11]. The magnetoresistance of the $x = 0.01$ sample at $T = 10$ K (the insulating regime) and of the $x = 0.02$ sample at $T = 200$ K (metallic conduction) are exhibited in the inset of figure 3. In the metallic regime, the magnetoresistance is small and positive.

The values obtained, typical of metallic compounds [20, 21], are slightly lower than the ones reported for $LaNiO_3$ [19]. In the insulating regime, the magnetoresistance is also low but negative, similar to what it is in other transition metal oxides [19]. Such behaviour may arise from weak-localization effects [22].

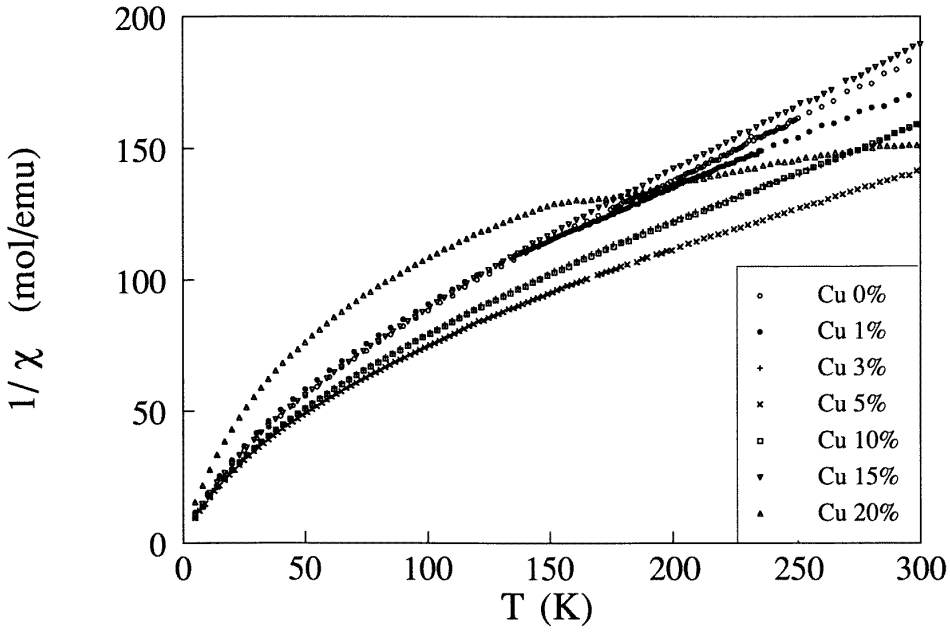

Figure 4. The inverse of the AC susceptibility versus temperature for $NdNi_{1-x}Cu_xO_3$ samples ($x \leqslant 0.2$).

Table 3. Magnetic parameters and calculated effective magnetic moments for $NdNi_{1-x}Cu_xO_3$ samples.

Sample (x)	C (emu K mol^{-1})	θ (K)	χ_0 (emu mol^{-1})	μ_{eff} (μ_B)
0	1.653	−60	0.9×10^{-3}	3.63
0.01	1.429	−58	1.8×10^{-3}	3.38
0.03	1.456	−39	2.05×10^{-3}	3.41
0.05	1.503	−42	2.7×10^{-3}	3.47
0.1	1.578	−46	1.8×10^{-3}	3.55
0.15	1.412	−41	1.2×10^{-3}	3.36

3.3. Magnetic properties

The inverse AC magnetic susceptibilities of $NdNi_{1-x}Cu_xO_3$ compounds are plotted in figure 4 as a function of temperature. All of the samples show a paramagnetic behaviour over the whole temperature range. Between 220 and 300 K, the curves have been fitted to $\chi = C/(T - \theta) + \chi_0$, where C and θ are the Curie and Weiss constants, respectively, and the χ_0-term corresponds to magnetic contributions independent of temperature such as Pauli

paramagnetism, Landau diamagnetism, core diamagnetism and Van Vleck paramagnetism. The behaviour of the $x = 0.2$ sample is slightly different, possibly due to the small amount of impurities seen in the XRD patterns. The values of parameters obtained from a least-squares fit are listed in table 3. All of the samples have similar effective magnetic moments which agree quite well with the value calculated for a free Nd^{3+} ion.

The positive sign of χ_0 indicates the importance of temperature-independent paramagnetic contributions to the total susceptibility in the samples studied. The Van Vleck and core parts can be estimated from the susceptibility data obtained for an insulating isomorphic $NdGaO_3$ sample [23]. Using these values and neglecting the much smaller contribution from the Landau diamagnetic term, we obtain a value of 2.11×10^{-3} emu mol^{-1} for the Pauli susceptibility of the $x = 0.05$ sample. This value is almost two orders of magnitude larger than the free-electron value. The enhancement of the susceptibility is somewhat smaller for other compositions. Nevertheless, this points to very strong correlations in perovskite nickelates.

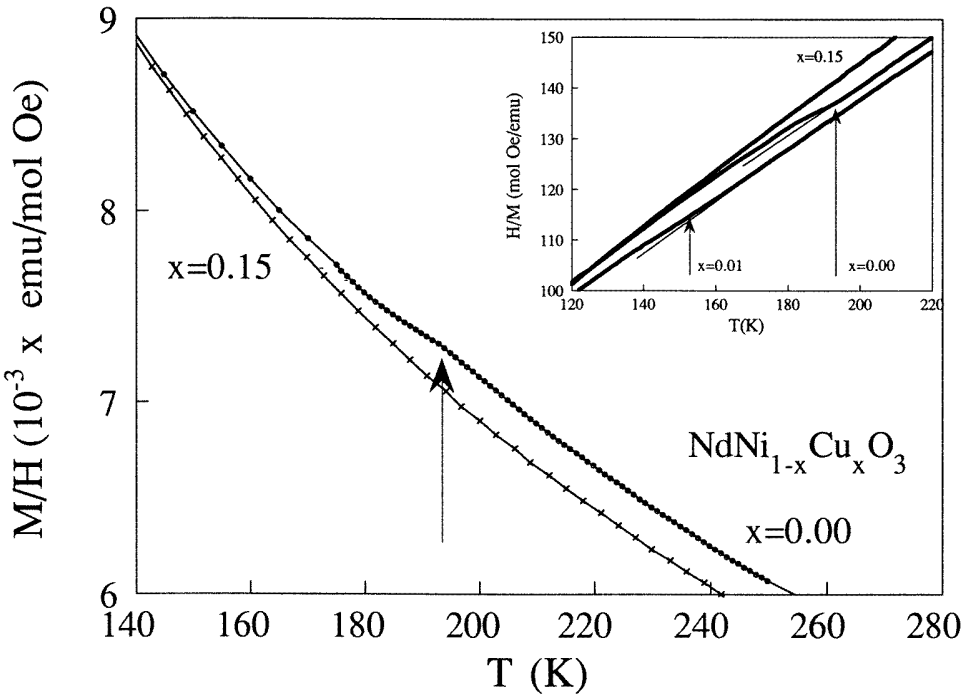

Figure 5. $\chi_{dc}(T)$ curves ($H = 2$ T) for $NdNi_{1-x}Cu_xO_3$ ($x = 0$ and 0.15) samples between 140 K and 260 K. The inset shows the inverse of χ_{dc} for samples with $x = 0.0$, 0.01 and 0.15 for the temperature range 120–220 K. The lines are guides to the eye. The MI transition temperatures are indicated by arrows.

The zero-field AC susceptibilities show a small kink at the MI temperature. However, the dc susceptibilities, measured in a field of 2 T, show clearly features related to the MI transition. Figure 5 shows the $1/\chi_{dc}(T)$ curve for $NdNiO_3$ and $x = 0.15$ samples. A clear anomaly in the behaviour of χ is seen at the MI transition temperature in samples with $x \leqslant 0.03$. Samples with metallic conduction do not show any anomaly in $\chi_{dc}(T)$. Therefore, we attribute the observed anomaly to the onset of a magnetic arrangement of

the Ni sublattice [8]. Accordingly, the substitution for Ni with Cu leads to simultaneous decreases in the temperature of the MI transition and in the temperature of the magnetic ordering. We note that in the absence of localization no magnetic ordering is produced.

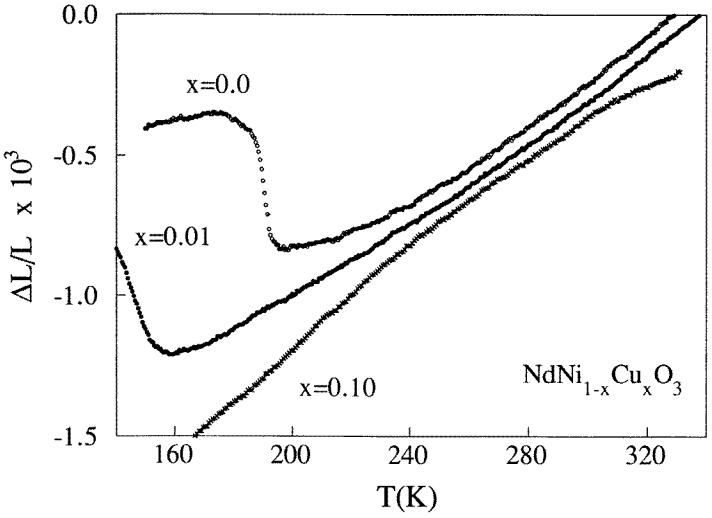

Figure 6. The linear thermal expansion of $NdNi_{1-x}Cu_xO_3$ ($x = 0$, 0.01 and 0.1) samples.

3.4. Linear thermal expansion

Figure 6 shows the linear thermal expansion of $x = 0, 0.01$ and 0.10 samples measured between 130 K and 340 K. For the $x = 0.1$ sample, which is metallic, the linear thermal expansion seems to be governed by the anharmonic phonon contribution. However, additional features are observed for the other two samples which show a jump in their $\Delta l/l$ curves. The $\Delta l/l$ change is larger for the $x = 0$ sample and the temperature at which the jump occurs correlates quite well with the MI transition temperature in both samples. Therefore we attribute this jump to the unit-cell expansion at the MI transition, as is also indicated by the neutron scattering experiments [7].

The high-temperature dilatation coefficient varies between 6.8×10^{-6} K^{-1} and 8.5×10^{-6} K^{-1} in the samples studied. It decreases slightly as Cu content increases.

3.5. Heat capacity

The experimental heat capacity of $NdNi_{1-x}Cu_xO_3$ with $x = 0$, 0.01 and 0.05 is shown in figure 7. A clear anomaly is observed at $T = 189$ K and at $T = 149$ K for the $x = 0$ and $x = 0.01$ samples, respectively. These values agree well with those obtained from resistivity and susceptibility anomalies. The $x = 0.05$ sample shows no anomaly over the whole temperature range as expected from transport and magnetic measurements. We note that the heat capacities of the samples studied are approximately equal near room temperature. In order to interpret the data, the lattice contribution to the specific heat has been assumed to be equal to the $LaGaO_3$ heat capacity, corrected by applying the corresponding-states law. The magnetic contribution, arising from the crystal-field splitting of the Nd^{3+} ground multiplet (the Schottky anomaly), has been calculated using the results obtained for $NdGaO_3$ [23]. In

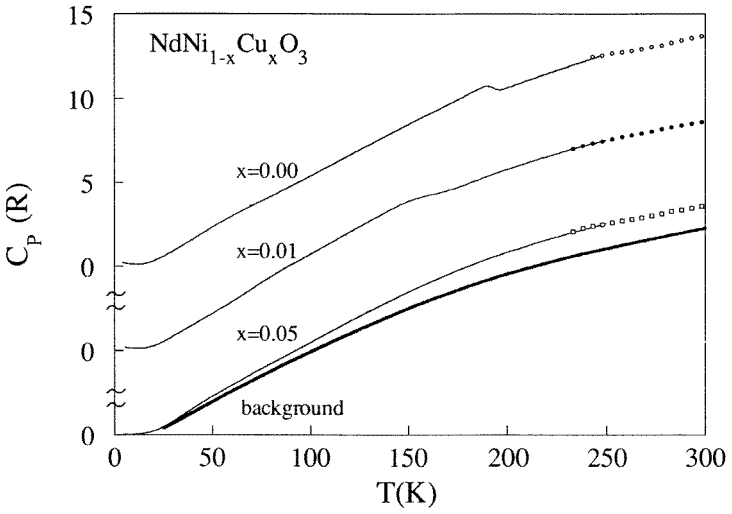

Figure 7. The heat capacity versus temperature of selected $NdNi_{1-x}Cu_xO_3$ samples.

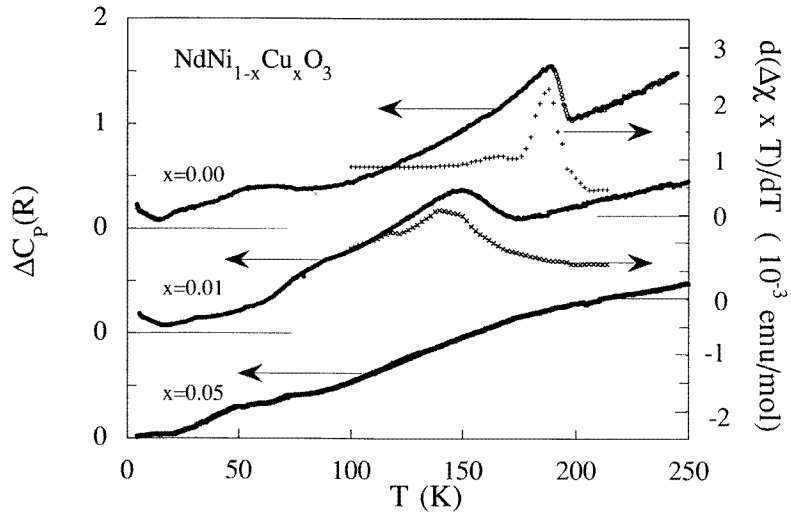

Figure 8. The excess heat capacity versus temperature for samples with $x = 0$, 0.01 and 0.05. The right-hand scale shows the values of $d(\Delta\chi\, T)/dT$, where $\Delta\chi = \chi(NdNi_{1-x}Cu_xO_3) - \chi(NdGaO_3)$ [23], for the $x = 0$ and $x = 0.01$ samples.

this way, we obtain the background (the sum of the lattice and Schottky contribution) heat capacity, shown by the continuous line in figure 7. The excess heat capacity, ΔC_p, which is the total heat capacity less the background contribution, is shown in figure 8. ΔC_p should be equal to the sum of the electronic and the magnetic (nickel sublattice ordering) heat capacities except for at low temperatures where an additional contribution arising from the splitting of the Nd^{3+} ground-state doublet may be observed [23]. Indeed, the heat capacity of the $x = 0$ and $x = 0.01$ samples increases with decreasing temperature for $T < 10$ K. This increase corresponds to the splitting of the Nd^{3+} ground-state doublet in the exchange

field arising from the interaction between the Nd and Ni sublattices [23]. Therefore, it provides clear evidence for the magnetic ordering of the Ni sublattice. The $x = 0.05$ sample, in which no magnetic order was seen, does not show such an increase. Its excess heat capacity varies almost linearly with temperature due to the electronic contribution. A least-squares fit to the relation $c = \gamma T$, in the temperature region where $T > 30$ K, yields a value of about 50 mJ mol^{-1} K^{-2} for the Sommerfeld constant. The free-electron value of γ, calculated assuming that each Ni atom contributes one electron, is equal to 1.41 mJ mol^{-1} K^{-2}. Therefore, a strong enhancement of the electronic contribution to the heat capacity is observed. The value of the effective mass of carriers, obtained from γ, is about 30 m_0 (m_0 is the free-electron mass). This is not far from the value estimated by optical spectroscopy (17 m_0) [24]. This strong enhancement of the effective mass is also in agreement with the large value of the Pauli susceptibility.

The magnetic entropy corresponding to the phase transition for $x = 0$ and $x = 0.01$ can be estimated by using in the integration of $\Delta C_p/T$ a smooth base-line from 100 K to 200 K and from 60 K to 180 K for $x = 0$ and $x = 0.01$, respectively. This procedure yields a value of $\Delta S = 0.12R$ and $\Delta S = 0.25R$ for $x = 0$ and $x = 0.01$, respectively, which agrees well with the results of DSC measurements [25]. The calculated values of the magnetic entropy are lower than the theoretical value expected for magnetic ordering of the spin $S = \frac{1}{2}$ (Ni^{3+}), indicating that large antiferromagnetic correlations exist in the metallic phase.

4. Discussion and conclusions

Our experimental results obtained for $NdNi_{1-x}Cu_xO_3$ perovskite oxides clearly show the complexity of this system. Let us summarize the most important experimental observations. The materials studied undergo a first-order temperature-driven MI transition. The temperature of this transition decreases linearly with increasing Cu content, so the samples with $x > 0.03$ are metallic for all temperatures. The MI transition is accompanied by a small unit-cell-volume increase although no changes are observed in the MO_6 octahedra which remain undistorted at room temperature for all of the compositions studied. Furthermore, there is no symmetry change. The onset of antiferromagnetic ordering in the Ni sublattice is observed at the MI transition. There is no magnetic ordering in the metallic material. External magnetic fields have a negligible effect on the MI transition and the magnetoresistance observed is very small. However, a very large enhancement of the Pauli susceptibility and of the electronic heat capacity is observed for all samples in the metallic regime. This clearly shows that the electron gas in $NdNi_{1-x}Cu_xO_3$ mixed oxides is highly correlated.

As we have shown, replacement of nickel by copper in $NdNiO_3$ compounds drastically changes their electrical transport properties. The substitution for 3% of nickel with copper suppresses the MI phase transition completely. We note that small composition modifications or application of an external pressure lead always to a metallic phase in nickel perovskites [9–11, 18]. It has been proposed that $NdNiO_3$ is a charge-transfer insulator in which the MI transition corresponds to the closing of the charge-transfer band gap [4]. This gap depends on how the tilts of NiO_6 octahedra are coupled and, therefore, on the Ni–O–Ni bond angle. The model cited explains qualitatively the relationship between the Ni–O–Ni bond angle and the MI phase transition temperature of the $RENiO_3$ and the $RE_{1-x}RE'_xNiO_3$ solid solutions [4, 17]. However, it cannot account for the effects of electron or hole doping or of the substitution other transition metals for nickel when no appreciable modification of the Ni–O–Ni bond angle is observed [10, 11]. The substitution of Fe or Co for Ni in $NdNiO_3$

produces the same effect as replacement with Cu although larger dopant concentrations are necessary to suppress the MI transition. In all cases, a light doping leads to the decrease of the MI transition temperature. We note that, in a simple band model, some of these dopants (e.g. Cu) put extra 3d electrons into the system while others subtract them. Nevertheless, in an ionic model, substituting Ni atoms for Cu or Fe atoms just modifies the atomic levels on some ions in the transition metal sublattice. Therefore, we do not expect any effect of doping on the Fermi level in this case.

Recent results of photoemission spectroscopy and electronic structure calculations point out the need to define the nickel perovskite oxides as covalent metals or insulators [3, 26] because of a large mixing of nickel 3d and oxygen 2p states in their ground state. X-ray absorption experiments performed on $NdNiO_3$ show similar 2p–3d-state mixing in the metallic and insulating phases [6]. This result implies that the Fermi level does not change across the MI transition. Therefore, a simple charge-transfer model, where the MI transition arises from the closing of the band gap between O 2p and Ni 3d bands, is not applicable in this case.

The MI transition in the oxides studied is complicated furthermore by a simultaneous antiferromagnetic ordering of Ni ions. Strong electron correlations give rise to an orbital superlattice in these materials [8]. Recently, an electronic localization produced by a charge ordering has been reported [27]. Such charge modulations arise from a strong phononic confinement (the polaron lattice) and are observed only for certain carrier concentrations at low temperatures. It seems quite plausible that a similar mechanism underlies the MI transition in $RENiO_3$ oxides. The substitution of Cu atoms for Ni atoms (as well as other replacements) would destroy the conditions necessary for developing orbital ordering and, consequently, would lead to the suppression of the MI transition.

Finally, we note that electronic correlations exist well above the MI transition temperature. The enhancement factors of the order of 30 which were obtained from the heat capacity data (and even larger values from the susceptibility data) cannot be explained by existing theories for nearly antiferromagnetic correlated metals [28]. We suggest that the formation of spin pseudoparticles [29], which is usually accompanied by charge polarization of the surrounding medium, would increase the effective-mass enhancement. We discard the possibility of the formation of ferromagnetic spin polarons which has been proposed for related manganese oxides [30] since no magnetoresistive effects are observed. In our case, we would expect an antiferromagnetic polaron, e.g. a quasiparticle with an antiferromagnetic correlation between spins [31], since the external magnetic field does not significantly affect their properties. Both the spin and the polarization fluctuations would contribute to the electron heavy mass in the metallic state and to its localization.

Acknowledgments

The authors acknowledge the financial support of the MAT96-0491 and MAT99-0804 projects.

References

[1] See for example
Goodenough J B 1971 *Prog. Solid State Chem.* **5** 276
Mott N F and Davis E A 1979 *Electronic Processes in Non-crystalline Materials* (Oxford: Clarendon)
[2] Zaanen J, Sawatzky G A and Allen J W 1985 *Phys. Rev. Lett.* **55** 418

[3] Mizokawa T, Namatame H, Fujimori A, Akeyama K, Kondoh H, Kuroda H and Kosugi N 1991 *Phys. Rev. Lett.* **67** 1638; 1994 *Phys. Rev.* B **49** 7193
[4] Torrance J B, Lacorre P, Nazzal A I, Ansaldo E I and Niedermayer C 1992 *Phys. Rev.* B **45** 8209
[5] Rajeev K P, Shivashankar G V and Raychaudhuri A K 1991 *Solid State Commun.* **79** 591
[6] García J, Blasco J, Proietti M G and Benfatto M 1995 *Phys. Rev.* B **52** 15 823
[7] García-Muñoz J L, Rodríguez-Carvajal J, Lacorre P and Torrance J B 1992 *Phys. Rev.* B **46** 4414
[8] García-Muñoz J L, Rodríguez-Carvajal J and Lacorre P 1992 *Europhys. Lett.* **20** 241; 1994 *Phys. Rev.* B **50** 978
[9] Alonso J A, Martínez-Lope M J and Hidalgo M A 1995 *J. Solid State Chem.* **116** 146
[10] Blasco J and García J 1994 *J. Phys. Chem. Solids* **55** 843
[11] Blasco J and García J 1994 *Solid State Commun.* **91** 381
[12] Blasco J, Castro M and García J 1994 *J. Phys.: Condens. Matter* **6** 5875
[13] Rodríguez-Carvajal J 1993 *Physica* B **192** 55
[14] Chen B-H, Walker D, Suard E, Scott B A, Mercey B, Hervieu M and Raveau B 1995 *Inorg. Chem.* **34** 2077
[15] Goodenough J B, Mott N F, Pouchard M and Demazeau G 1973 *Mater. Res. Bull.* **8** 647
[16] García-Muñoz J L, Suaaidi M, Martínez-Lope M J and Alonso J A 1995 *Phys. Rev.* B **52** 13 563
[17] Blasco J and García J 1994 *J. Phys.: Condens. Matter* **6** 10 759
[18] Canfield P C, Thompson J D, Cheong S-W and Rupp L W 1993 *Phys. Rev.* B **47** 12 357
Obradors X, Paulius L M, Maple M B, Torrance J B, Nazzol A J, Fontcuberta J and Granados X 1993 *Phys. Rev.* B **47** 12 353
[19] Raychaudhuri A K 1995 *Adv. Phys.* **44** 21
[20] Ziman J M 1963 *Electrons and Phonons* (Oxford: Clarendon)
[21] Isawa K, Sugiyama J and Yamauchi H 1993 *Phys. Rev.* B **47** 11 426
[22] Kawabata A 1980 *Solid State Commun.* **34** 431
Lee P A and Ramakrishnan T V 1985 *Rev. Mod. Phys.* **57** 287
[23] Bartolomé F, Kuz'min M D, Bartolomé J, Blasco J, García J and Sapiña F 1994 *Solid State Commun.* **91** 177
Bartolomé F 1995 *PhD Thesis* University of Zaragoza
[24] Katsufuji T, Okimoto Y, Arima T and Tokura Y 1995 *Phys. Rev.* B **51** 4830
[25] Granados X, Fontcuberta J, Obradors X, Mañosa Ll and Torrance J B 1993 *Phys. Rev.* B **48** 11 666
[26] Mizokawa T, Fujimori A, Arima T, Tokura Y, Mori N and Akimitsu J 1995 *Phys. Rev.* B **52** 13 865
[27] Chen C H, Cheong S-W and Cooper A S 1993 *Phys. Rev. Lett.* **71** 2461
[28] Brinkman W F and Rice T M 1971 *Phys. Rev.* B **4** 1566
[29] von Molnar S, Briggs S, Flouquet J and Remenyi G 1983 *Phys. Rev. Lett.* **57** 706
[30] von Helmolt R, Wecker J, Holzapfel B, Schultz L and Samwer K 1993 *Phys. Rev. Lett.* **71** 2331
[31] Nagaev E L 1983 *Physics of Magnetic Semiconductors* (Moscow: MIR) p 307